

Roles of Toroidal Rotation at the Plasma Edge, Toroidal Field Ripple and Configuration on ELMs in the JT-60U Tokamak

Kensaku KAMIYA, Hajime URANO, Naoyuki OYAMA and Yutaka KAMADA

Japan Atomic Energy Agency, Naka, Ibaraki 311-0193, Japan

(Received 13 December 2006 / Accepted 24 January 2007)

Recent experimental studies are presented regarding ELMy H-mode plasma having Type-I Edge Localized Modes (ELMs) in the JT-60U. Toroidal rotation scan experiments in inward-shifted, small-volume plasma show that the ELM energy loss decreases as the toroidal rotation at the plasma edge increases in the direction counter to the plasma current. Specifically for a large volume plasma having a toroidal field ripple of $\sim 2\%$ at the plasma edge, small Type-I ELMs are observed whose ELM energy loss normalized by the pedestal stored energy is smaller than that of an acceptable ELM size in the ITER. However, the pedestal pressure tends to decrease when plasma volume increases. No remarkable effect of reduced toroidal field ripple due to the installation of Ferritic Steel Tile (FSTs) inside the vacuum vessel on the JT-60U on ELMs for large volume plasma is seen in the ELM energy loss normalized by the pedestal stored energy. These new findings suggest that the toroidal field ripple itself may not directly affect the normalized ELM energy loss, and that toroidal rotation at the plasma edge as well as plasma configuration might play important roles in the prediction of ELM size in future devices.

© 2007 The Japan Society of Plasma Science and Nuclear Fusion Research

Keywords: ELM, H-mode, tokamak, ITER, divertor, plasma rotation, toroidal field ripple, plasma configuration

DOI: 10.1585/pfr.2.005

1. Introduction

High confinement mode (H-mode) operation having an Edge Localized Mode (ELM) is a candidate for the reference inductive operational scenario for the ITER (e.g., a ratio of the fusion power to the additional heating power, $Q_{DT} = 10$) [1]. One of the most remarkable phenomena in the H-mode plasmas having Type-I ELMs (so-called, “Type-I” ELMy H-mode) is the large and periodic power and particles directed toward the divertor and/or the first-wall, which is normally observed for the best performing H-mode in many tokamaks. For the ITER reference inductive scenario in ELMy H-mode operation, periodic ELM crash and recovery have a potential for controlling plasma density and impurity accumulation in the plasma core, which is essential for a steady state operation, though ELMs induced energy and particle losses can potentially limit the divertor’s lifetime (e.g., an acceptable divertor lifetime could be realized only by an upper limit of ELM energy loss normalized by pedestal stored energy, $\Delta W_{ELM}/W_{ped} \sim 5\text{-}6\%$ [2]).

Approaches to controlling the Type-I ELMs, such as “Ergodization” on DIII-D [3], “Pace making by a shallow pellet injection” on ASDEX-Upgrade [4], and “Vertical motion” on TCV [5], have been successfully demonstrated in many tokamaks. On the other hand, finding alternative scenarios to Type-I ELMy H-mode operation also constitutes a key area of research for current tokamaks. Specifically, the “Quiescent H-mode (QH-mode)” on DIII-D [6]

(recently, reproduced on the ASDEX-Upgrade [7] and the JT-60U [8, 9]), and “Grassy ELMs” on the JT-60U [9, 10] demonstrated high confinement (being comparable to that of Type-I ELMy H-mode plasmas at similar parameters) in the absence of large, ELMs induced, transient heat/particle fluxes onto the divertor targets. These plasmas show a toroidal rotation at the plasma edge, $v_{T,ped}$, in the direction counter to the plasma current, providing a controllable parameter through which ELMs can be controlled, though underlying physics of this phenomenon is not yet well understood. Furthermore, the behavior of ELMs with the change in the power of neutral beam injection (NBI) in the JT-60U exhibited a complex nature, since the negative radial electric field, E_r , formation due to losses of fast ions originating mainly from the perpendicular NBI as well as the $v_{T,ped}$ could vary with external momentum input from tangential NBI [11, 12].

The goal of this research area is to understand the roles of the toroidal rotation at the plasma edge, toroidal field ripple (TF-ripple), and configuration in ELM energy loss. The physics which can determine the edge processes may offer a key to develop an operational scenario in future devices. This paper presents a systematic study of the Type-I ELM characteristics in tangential co-, balanced-, and counter-NBI plus perpendicular NBI-heated plasmas with various configurations. In this study, the ELM characteristics are related to the change in the toroidal rotation at the plasma edge, TF-ripple, and plasma configuration.

This paper is organized as follows. Section 2 con-

author’s e-mail: kamiya.kensaku@jaea.go.jp

tains a brief description of the neutral beam injection (NBI) heating system and diagnostics of the JT-60U. Section 3 characterizes the effects of toroidal rotation at the plasma edge on ELMs in inward-shifted, small-volume plasma. The effects of toroidal field ripple and/or plasma configurations on ELMs, in addition to new findings after the installation of Ferritic Steel Tiles (FSTs) inside the vacuum vessel of the JT-60U, are also presented. In Sec. 4, a comparison with the international database of ELM energy loss in many tokamaks is discussed. Finally, Sec. 5 summarizes this study, in terms of current qualitative understanding of ELMs in addition to the related issue.

2. Apparatus

The JT-60U has 11 positive-ion-based Neutral Beams (PNBs ~ 85 keV) and 2 negative-ion-based NBs (NNBs ~ 350 -420 keV, #15 and #16) as shown in Fig. 1. There are two tangential co-NBIs (#9 and #10) and two ctr-NBIs (#7 and #8), while the other 7 units are nearly perpendicular NBIs, which provide wide variations in the combination of tangential (co/bal/ctr) and perpendicular injection. In this study, the tangential NBIs are utilized for the rotation scans (e.g. co-, balanced- and counter-NBIs), and the perpendicular-NBIs are added to increase the heating power. No NNB is used for this study. As shown in Fig. 2, the electron density, n_e , and temperature, T_e , can be measured on the JT-60U by use of Thomson scattering. Also, ion temperature, T_i , and toroidal rotation, v_T , profiles can be measured by use of Charge eXchange Recombination Spectroscopy (CXRS) from poloidal and toroidal viewing geometries, respectively. The energy lost from the core plasma due to an ELM can be measured on the JT-60U by the use of a diamagnetic loop diagnostic with a time resolution of ~ 250 μ s.

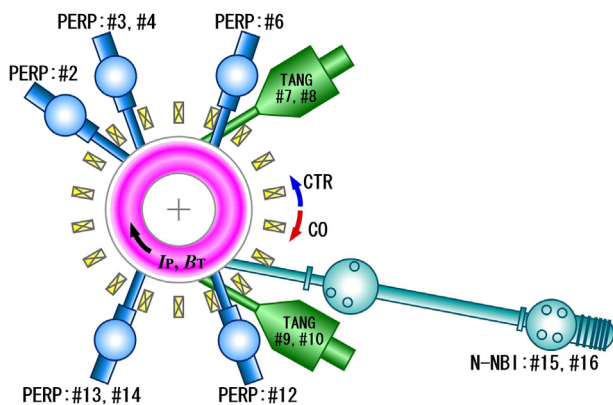


Fig. 1 Top view of the JT-60U torus, showing the NBI heating system.

3. Experimental Results

3.1 Effect of toroidal rotation at the plasma edge on ELMs

A rotation scan experiment was performed under the following plasma parameters: plasma current, $I_P = 1.0$ MA and toroidal magnetic field, $B_T = 2.6$ T ($q_{95} \sim 4$) at the $\bar{n}_e/n_{GW} \sim 0.4$ -0.5, scanning combinations of NBI in the inward-shifted and small plasma volume, $V_P \sim 50$ m³. The magnetic equilibria ($\delta \sim 0.24$, $\kappa \sim 1.59$ and $\beta_P \sim 1.41$) for the discharges of this study is also shown in Fig. 2. Here, \bar{n}_e/n_{GW} is the line-averaged electron density, \bar{n}_e , normalized by Greenwald density, $n_{GW} (= I_P/\pi a^2$ in units of 10^{20} m⁻³, where a is the plasma minor radius in [m]), q_{95} is the safety factor at the surface containing 95% of the magnetic flux, δ is triangularity, κ is elongation, and β_P is poloidal beta.

The ELM's global effects are shown in Fig. 3. It is found that the ELM frequencies, f_{ELM} , increase due to the stepped increase in the heating power from the perpendicular NBI during each discharge. Figure 4 shows an expanded view of the time evolution of the stored energy, W_{dia} , (solid lines) and D_α emission (dotted lines) during ELM cycles ($\Delta T = 100$ ms) at the heating power crossing the separatrix, $P_{SEP} \sim 6$ MW ($\equiv P_{ABS} - P_{RAD} - dW/dt$). Here, P_{ABS} is the absorbed power, P_{RAD} radiation loss power, and dW/dt the increased rate of the total energy stored in the plasma. The tangential- plus perpendicular-NBI heated plasmas in "small" volume plasmas indicate that smaller and more frequent ELMs are seen in the counter-NBI discharge than in the co-NBI discharge. Balanced-NBI discharge is intermediate between them. It

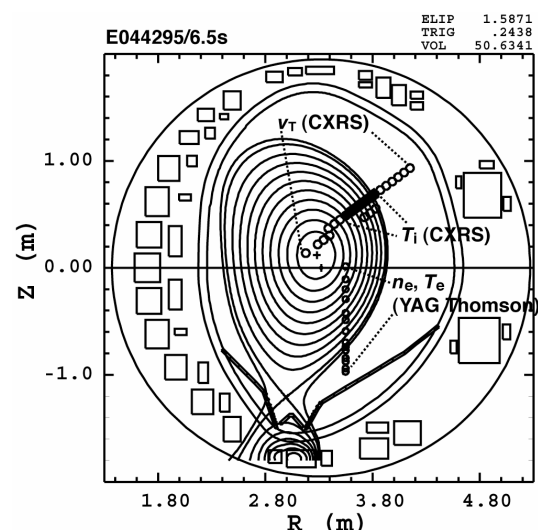


Fig. 2 Poloidal cross-sectional view of the JT-60U. Also shown are the YAG Thomson scattering (electron density and temperature) and Charge eXchange Recombination Spectroscopy (CXRS, edge ion temperature from poloidal view and toroidal rotation from toroidal view) measurement locations.

should be noted that all data presented here could be classified into “Type-I” ELMs according to the well-known dependence of the f_{ELM} on the P_{SEP} , as $df_{\text{ELM}}/dP_{\text{SEP}} \geq 0$ as shown in Fig. 5. Each data point in Fig. 5 represents the averaged value during ELM cycles over an interval of $\Delta t \sim 100$ ms, and the corresponding error bar is

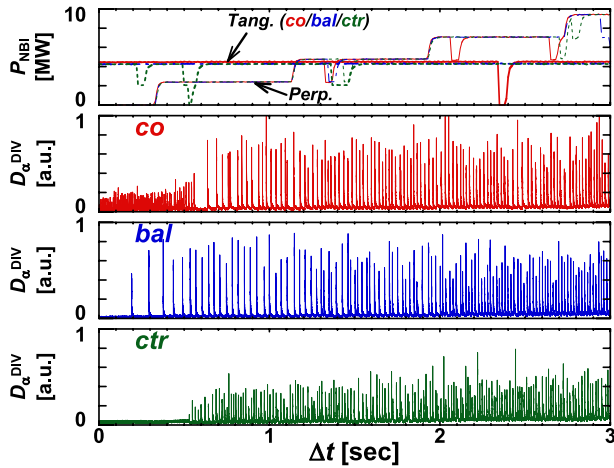


Fig. 3 ELMy H-mode discharges having Type-I ELMs on the JT-60U for inward-shifted and “small” volume plasmas (plasma volume $V_p \sim 50 \text{ m}^3$); (a) NBI power, (b) ELM activities seen in the D_α signal from the chord viewing divertor region for the tangential co- (red line), (c) balanced- (blue line), and (d) counter- (green line) plus perpendicular-NBI heated plasmas. Horizontal axes at each column are adjusted to the NBI waveform, respectively.

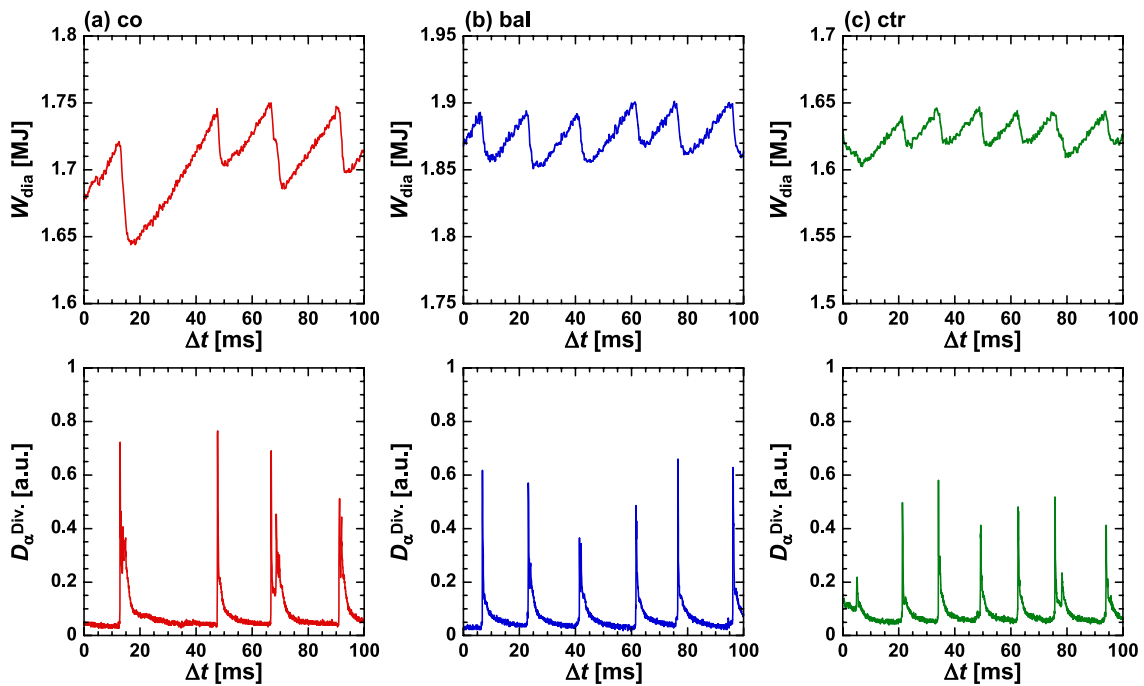


Fig. 4 Expanded view of the time evolution of the stored energy (top) and D_α emission (bottom) during ELM cycles ($\Delta t = 100$ ms) at the heating power crossing the separatrix of $P_{\text{SEP}} \sim 6 \text{ MW}$ for the tangential (a) co- (red line), (b) balanced- (blue line), and (c) counter- (green line) plus perpendicular-NBI heated plasmas in “small” volume plasmas.

the standard deviation of this averaging process. A detailed comparison of the power dependences of the f_{ELM} , $df_{\text{ELM}}/dP_{\text{SEP}}$ among co-, balanced and counter-NBI discharges shows that not only the P_{SEP} , but also the variation in the external momentum input (i.e., co-, balanced- and counter-NBI) could affect the ELM characteristics. A comparison of co-, balanced- and counter-NBI discharges at a given $P_{\text{SEP}} \sim 6 \text{ MW}$ shown in Fig. 6 results that toroidal rotation at the top of the pedestal, $v_{T,\text{ped}}$, varies widely from 20 km/s in co-NBI to -80 km/s in counter-NBI, while no significant degradation appears in the pedestal pressures for the counter-NBI discharge, except for a slightly higher electron density at the top of the pedestal seen in the co-NBI discharge. In addition, it should be noted that slight differences in the pedestal height/width could not be identified due to diagnostic restrictions in this study, especially for the electron density and temperature profiles. A detailed comparison of these factors is left for future study.

Figure 7 shows the correlation of ELM energy loss normalized by the stored energy at the pedestal region, $\Delta W_{\text{ELM}}/W_{\text{ped}}$, with the $v_{T,\text{ped}}$, while the inverse-correlation of the f_{ELM} with the $v_{T,\text{ped}}$ can be seen at a given $P_{\text{SEP}} \sim 6 \text{ MW}$, keeping the ELM exhaust power, $P_{\text{ELM}} (\equiv f_{\text{ELM}} \times \Delta W_{\text{ELM}})$, almost constant. The change in the normalized ELM energy loss, $\Delta W_{\text{ELM}}/W_{\text{ped}}$, is about 25% when the $v_{T,\text{ped}}$ is widely changed from 20 km/s in co-NBI to -80 km/s in counter-NBI, while the change in the p_{ped} is about 15%. A significant toroidal rotation at the plasma edge in the direction counter to the plasma current (e.g. $|v_{T,\text{ped}}| \sim 50\text{-}100$ km/s on JT-60U, typically) could provide

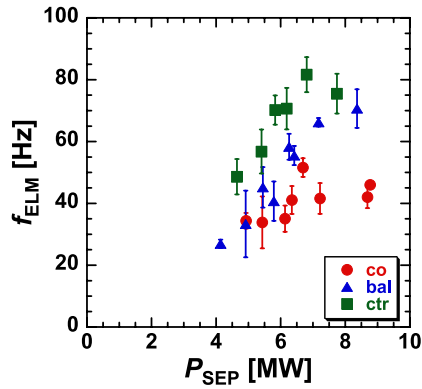


Fig. 5 Plots of ELM frequency, f_{ELM} , versus heating power crossing the separatrix, P_{SEP} , in the tangential in the tangential co- (full circles), balanced- (full triangles), and counter- (full squares) plus perpendicular-NBI heated plasmas plus perpendicular-NBI heated plasmas for “small” volume plasmas ($V_p \sim 50 \text{ m}^3$).

a controllable parameter for ELM mitigation, if the toroidal rotation could be controlled only at the plasma edge region without any confinement degradation at the plasma core region [13]. However, the direct application of this ELM mitigation technique to the ITER condition is still uncertain, since it requires further reduction of ELM energy loss (e.g., a factor ~ 2 or more reduction from the typical predicted value of Type-I ELM) without any confinement degradation.

3.2 Effects of toroidal field ripple on ELMs

In the JT-60U, it is well known that a significant $v_{T,\text{ped}}$ in the direction counter to the plasma current has been observed as an offset toroidal rotation in the plasma’s peripheral region even in the co-NBI (+ perp.) discharge at a given P_{SEP} as shown in Fig. 8, which is related to the losses of fast ions due to perpendicular NBI and the formation of negative E_r [11, 12]. From the results described above, it

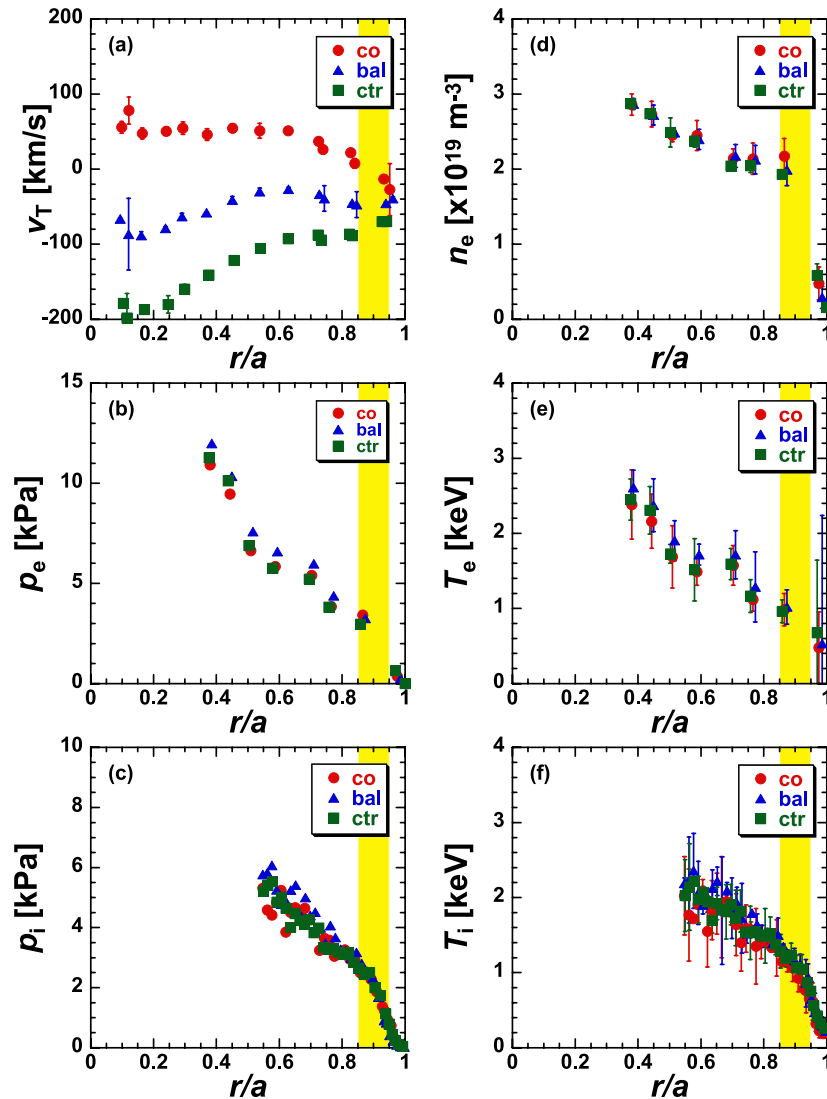


Fig. 6 Profiles of (a) toroidal rotation, (b) electron pressure, (c) ion pressure, (d) electron density, (e) electron temperature, and (f) ion temperature are plotted against the normalized radius, r/a , in the tangential co- (full circles), balanced- (full triangles), and counter- (full squares) plus perpendicular-NBI heated plasmas at a given $P_{\text{SEP}} \sim 6 \text{ MW}$ for “small” volume plasmas ($V_p \sim 50 \text{ m}^3$).

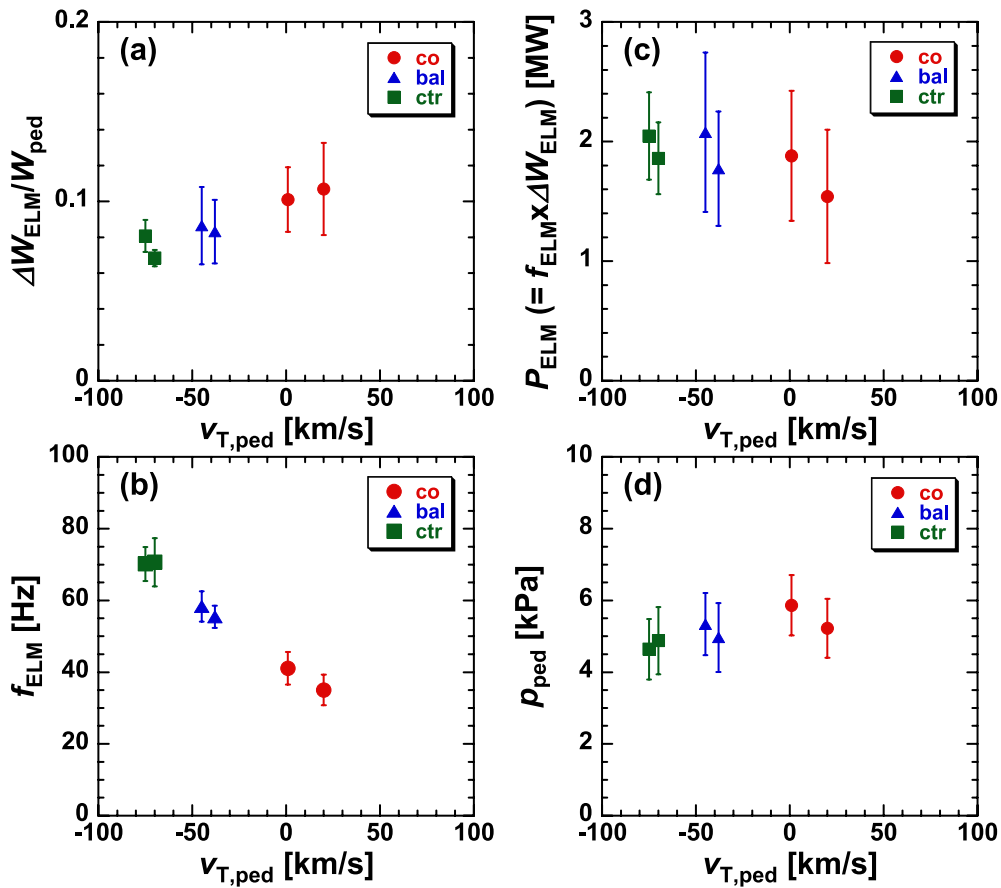


Fig. 7 (a) ELM energy loss normalized by the pedestal stored energy, $\Delta W_{\text{ELM}}/W_{\text{ped}}$, (b) ELM frequency, f_{ELM} , (c) ELM exhaust power, $P_{\text{ELM}} (\equiv f_{\text{ELM}} \times \Delta W_{\text{ELM}})$, and (d) pedestal pressure, p_{ped} , plotted against the toroidal rotation at the top of the pedestal, $v_{\text{T,ped}}$, in the tangential co- (full circles), balanced- (full triangles), and counter- (full squares) plus perpendicular-NBI heated plasmas at a given $P_{\text{SEP}} \sim 6$ MW for “small” volume plasmas ($V_{\text{P}} \sim 50$ m³).

is suggested that the effect of the resultant toroidal rotation at the plasma edge caused by the losses of the fast ions due to the TF-ripple on ELMs is also an interesting edge phenomenon, which may also provide a controllable parameter for ELM mitigation.

TF-ripple scan experiments were performed on configurations having TF-ripples at the plasma edge, δ_{ripple} , of $\sim 0.4\%$ (small $V_{\text{P}} \sim 50$ m³), $\sim 1.0\%$ (middle $V_{\text{P}} \sim 65$ m³), and $\sim 2\%$ (large $V_{\text{P}} \sim 75$ m³) under the condition of the $I_{\text{P}} = 1.0$ MA (small), 1.1 MA (middle), and 1.2 MA (large) at a fixed $B_{\text{T}} = 2.6$ at a $n_{\text{e}}/n_{\text{GW}} \sim 0.4$ -0.5, scanning combinations of tangential NBI and heating power of perpendicular NBI. The magnetic equilibria with $\delta/\kappa \sim 0.24/1.59$, $\sim 0.35/1.45$ and $\sim 0.33/1.40$ for the discharges of the small, middle, and large V_{P} configurations, respectively, are shown in Fig. 9. It is noted that the q_{95} at each configuration is almost the same value of ~ 4 due to an increased I_{P} in the case of a larger plasma volume (or surface area).

Figure 10(a) shows a close correlation of $\Delta W_{\text{ELM}}/W_{\text{ped}}$ with a $v_{\text{T,ped}}$ under a $P_{\text{SEP}} \sim 5$ -6 MW at each configuration, showing similar slopes in the dependence of $\Delta W_{\text{ELM}}/W_{\text{ped}}$ on $v_{\text{T,ped}}$. A reason for the narrower dynamic range toward the co-direction in the

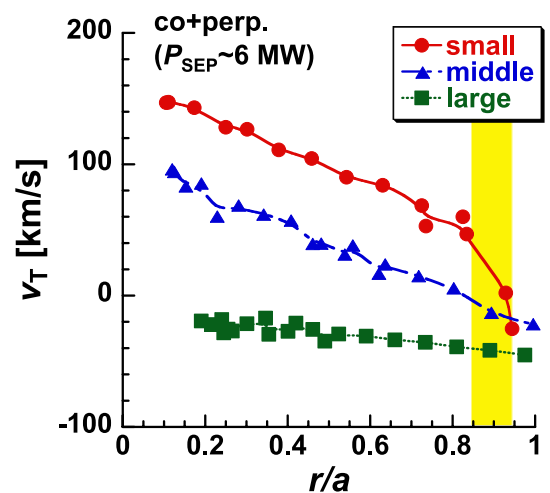


Fig. 8 Profiles of toroidal rotation are plotted against the normalized radius, r/a , in the co-NBI (plus perpendicular NBI) discharges at a given $P_{\text{SEP}} \sim 6$ MW for configurations having a toroidal field ripple of $\delta_{\text{ripple}} \sim 0.4\%$ (circles, small $V_{\text{P}} \sim 50$ m³), 1.0% (triangles middle $V_{\text{P}} \sim 65$ m³), and 2% (squares, large $V_{\text{P}} \sim 75$ m³).

$v_{T,ped}$ for the larger volume configuration is due to an offset toroidal rotation towards the counter-direction at the plasma's edge region due to larger losses of fast ions from perpendicular NBI [11–13]. As shown in Fig. 10(b), the power fraction lost by fast ions is less than 15% in the configuration having small plasma volume, while it is more than 30% in the configuration having a large plasma volume. Here, the power fraction lost by fast ions is defined as $(P_{orbit} + P_{ripple} + P_{CX})/(P_{NBI} - P_{ST})$, which is the sum of the powers of the orbit loss, P_{orbit} , ripple loss, P_{ripple} , and charge exchange loss, P_{CX} , normalized by the NBI power, P_{NBI} , from which shine-through power, P_{ST} ,

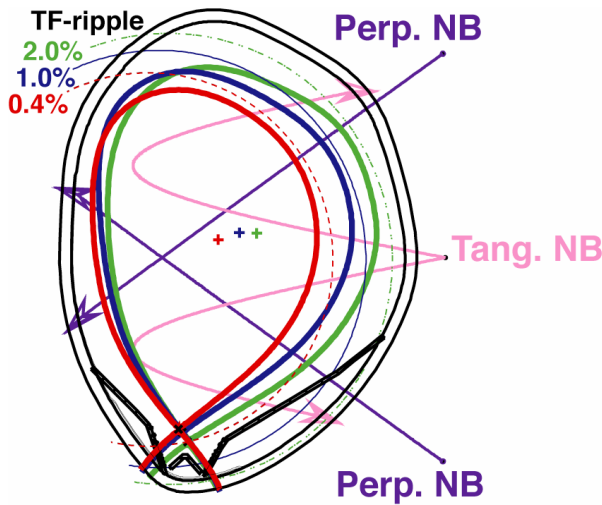


Fig. 9 The magnetic equilibria with $\delta/\kappa \sim 0.24/1.59$, $\sim 0.35/1.45$, and $\sim 0.33/1.40$ for discharges of small $V_p \sim 50 \text{ m}^3$, middle $V_p \sim 65 \text{ m}^3$, and large $V_p \sim 75 \text{ m}^3$ configurations, respectively. The contours of toroidal field ripples δ_{ripple} of 0.4% (small $V_p \sim 50 \text{ m}^3$), 1.0% (middle $V_p \sim 65 \text{ m}^3$), and 2% (large $V_p \sim 75 \text{ m}^3$) are also shown.

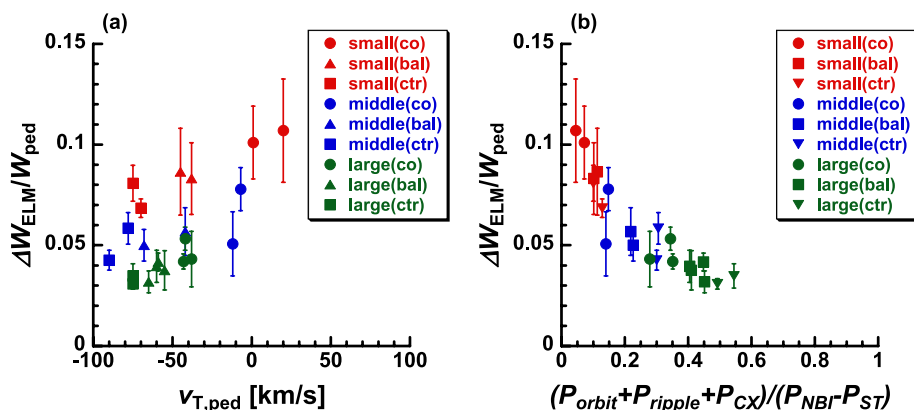


Fig. 10 ELM energy loss normalized by the pedestal stored energy, $\Delta W_{ELM}/W_{ped}$, plotted against (a) toroidal rotation at the top of the pedestal, $v_{T,ped}$, and (b) the power fraction lost by fast ions in the tangential co- (full circles), balanced- (full triangles), and counter- (full squares) plus perpendicular-NBI heated plasmas at a $P_{SEP} \sim 5\text{--}6 \text{ MW}$ for the configurations having toroidal field ripples of $\delta_{ripple} \sim 0.4\%$ (red; small $V_p \sim 50 \text{ m}^3$), 1.0% (blue; middle $V_p \sim 65 \text{ m}^3$), and 2% (green; large $V_p \sim 75 \text{ m}^3$), respectively. The power fraction lost by fast ions are defined as $(P_{orbit} + P_{ripple} + P_{CX})/(P_{NBI} - P_{ST})$, which is the sum of the powers of the orbit loss, P_{orbit} , ripple loss, P_{ripple} , and charge exchange loss, P_{CX} , normalized by the NBI power, P_{NBI} , from which shine-through power, P_{ST} , is subtracted.

is subtracted.

The most important point in Fig. 10(a) is a systematic difference in the $\Delta W_{ELM}/W_{ped}$ (in other words, offset $\Delta W_{ELM}/W_{ped}$) varying from $\sim 9\%$ (small-volume), $\sim 6\%$ (middle-volume), and $\sim 4\%$ (large-volume) at a given $v_{T,ped} \sim -50 \text{ km/s}$, suggesting important roles of other parameters in determining the edge stability, such as TF-ripple, losses of fast ions, and plasma configuration. It should be noted that the pedestal pressure and/or poloidal beta, $\beta_{p,ped}$, tends to decrease when plasma volume increases [13]. However, the decrease in ΔW_{ELM} is larger than that seen in W_{ped} , and hence $\Delta W_{ELM}/W_{ped}$ decreases when plasma volume or δ_{ripple} increases.

3.3 Effects of reduced TF-ripple on ELMs

Recent experiments run on the JT-60U have successfully demonstrated a reduction of the toroidal field ripple after the installation of Ferritic Steel Tiles (FSTs) inside the vacuum vessel. One of the advantages of H-mode studies in the JT-60U is that a comparison between the pre- and the post-FSTs campaigns makes it possible to clarify the effects of reduced TF-ripple on ELMs and the pedestal under the matched plasma configurations as shown in Fig. 11, eliminating uncertainties in the shaping effect.

As reported in Ref. [14], an enhanced $v_{T,ped}$ into the co-direction due to reduced losses of fast ions from perp.-NBI is clearly observed after the installation of FSTs only at the specific configurations (large $V_p \sim 75 \text{ m}^3$) shown in Fig. 11, and the p_{ped} tends to increase with $v_{T,ped}$. The result from the calculation using the Fully Three-Dimensional magnetic field Orbit-Following Monte-Carlo (F3D OFMC) code [15] shows that the power fraction lost by fast ions, which is defined as $(P_{orbit} + P_{ripple} + P_{CX})/(P_{NBI} - P_{ST})$, is reduced from 30–40% in the pre-FSTs campaign to 15–20% in the post-FSTs campaign in

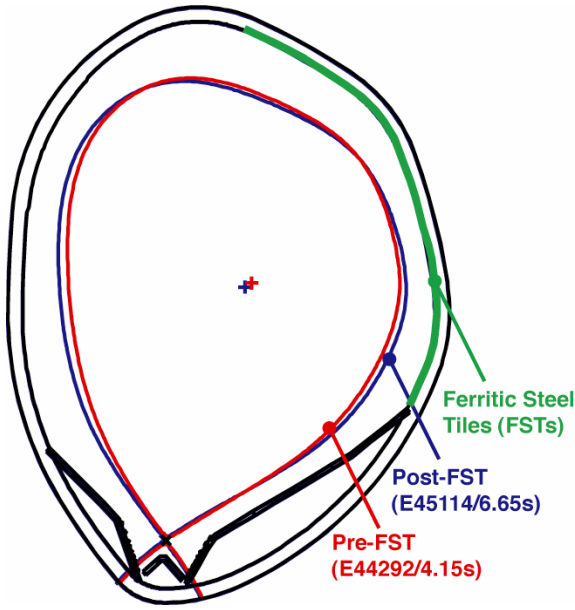


Fig. 11 Poloidal cross-sectional view of the JT-60U, comparing pre- and post-FSTs campaigns for “large” volume plasmas ($V_p \sim 75 \text{ m}^3$). The locations of the FSTs are also shown.

the configuration having large plasma volume with co-tangential plus perpendicular-NBI discharges. Furthermore, compared to the pre- and the post-FSTs campaigns, a higher p_{ped} is obtained in the case with FSTs even at a given $v_{T,\text{ped}}$, again. The extended width of the H-mode pedestal with enhanced $v_{T,\text{ped}}$ into the co-direction and a reduced TF ripple are also clearly demonstrated after installation of FSTs only at the specific configurations (large $V_p \sim 75 \text{ m}^3$) shown in Fig. 11. These experimental results are obtained by a systematic comparison between the pre- and the post-FSTs campaigns at a matched plasma shape with almost the same wall conditions, eliminating uncertainties regarding both the shaping effect and neutral recycling. So far, no significant enhanced pedestal performances, such as higher pedestal height and/or wider pedestal width, have been achieved in other configurations (e.g., small and middle volume cases).

A comparison of the pre- and post-FSTs campaigns shows that they share a similarity regarding the dependence of $\Delta W_{\text{ELM}}/W_{\text{ped}}$ on $v_{T,\text{ped}}$ as shown in Fig. 12. This is because both ELM energy loss ΔW_{ELM} and pedestal stored energy W_{ped} increase according to the enhanced $v_{T,\text{ped}}$ toward the co-direction, and hence, dependences of the normalized ELM energy loss $\Delta W_{\text{ELM}}/W_{\text{ped}}$ on $v_{T,\text{ped}}$ remain unchanged even after FSTs installation. So, it is suggested that the role of “configuration” is more important than δ_{ripple} in the appearance of small Type-I ELM in large volume plasma, and the TF-ripple itself and/or losses of fast ions may not be directly related to the normalized ELM energy loss, $\Delta W_{\text{ELM}}/W_{\text{ped}}$.

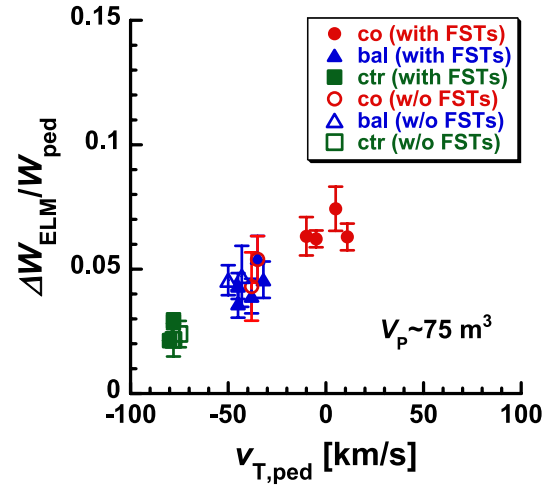


Fig. 12 A comparison of pre- and post-FSTs campaigns in terms of ELM energy loss normalized by the stored energy in the pedestal region, $\Delta W_{\text{ELM}}/W_{\text{ped}}$, plotted against the toroidal rotation at the top of the pedestal, $v_{T,\text{ped}}$, in the tangential co- (circles), balanced- (triangles), and counter- (squares) plus perpendicular-NBI heated plasmas at $P_{\text{SEP}} \sim 5 \text{ MW}$ for the configuration having large plasma volume ($V_p \sim 75 \text{ m}^3$).

4. Comparison of ELM Energy Loss with the International Database

For configurations having small and large plasma volumes, respectively, Figs. 13 (a) and (b) show a comparison with the international database for the Type-I ELM energy loss normalized by pedestal stored energy, $\Delta W_{\text{ELM}}/W_{\text{ped}}$, which is plotted against collisionality, ν_e^* ($\propto n_e R q_{95} / \varepsilon^{3/2} T_e^2$), at the top of the pedestal [2]. Looking at the data in terms of DIII-D (circles), JET (triangles), and ASDEX-Upgrade (squares), a close correlation of $\Delta W_{\text{ELM}}/W_{\text{ped}}$ with edge collisionality can be seen, and small ELM energy loss is revealed only at a high collisionality regime of around $\nu_e^* \geq 1$. The physical mechanism of this phenomenon may be contained in the peeling-ballooning model for the ELM together with the influence of collisionality on the edge bootstrap current and change in the associated MHD unstable mode structure [16]. In the ITER, ν_e^* is estimated to be ~ 0.06 as identified by the vertical dotted line in Figs. 13 (a) and (b). The expected maximum tolerable ELM size in the ITER of around $\Delta W_{\text{ELM}}/W_{\text{ped}} \sim 5\text{-}6\%$ is also shown in the hatched area [17, 18]. Using this scaling, one can extrapolate the $\Delta W_{\text{ELM}}/W_{\text{ped}}$ of the present experiments to the ITER, although there is a large variation in the $\Delta W_{\text{ELM}}/W_{\text{ped}}$ even at fixed collisionality (e.g., the variation in the $\Delta W_{\text{ELM}}/W_{\text{ped}}$ is from 13% up to 20% at the ITER ν_e^*). Thus, based on the present experiments, the extrapolation of the ELM energy loss to the ITER remains uncertain.

As described in Sec. 3.1, the ELM energy loss can be controlled by means of counter-NBI in a clear Type-I ELM

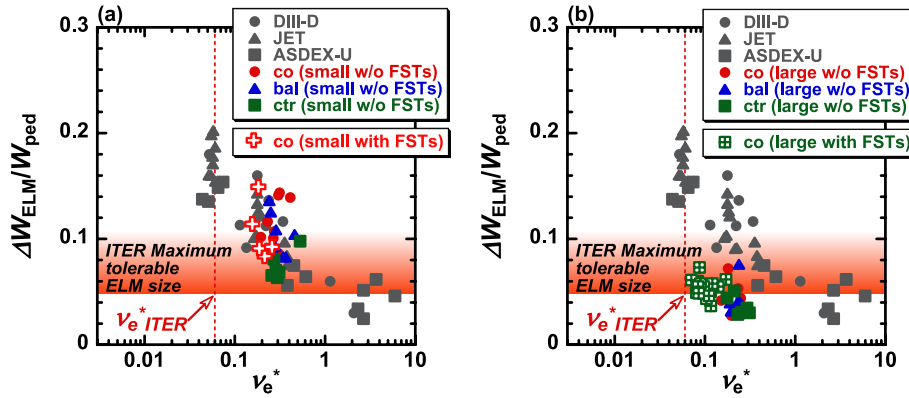


Fig. 13 Normalized ELM energy loss, $\Delta W_{ELM}/W_{ped}$, versus pedestal plasma collisionality, ν_e^* , for a large range of Type-I ELMy H-mode plasmas in the DIII-D (circles), the JET (triangles), and ASDEX-U (squares) shown in gray colors, including various plasma triangularities, ratios of the input power to the threshold power, $P_{INPUT}/P_{L/H}$ and pellet triggered ELMs. (a) The database of $\Delta W_{ELM}/W_{ped}$ in the toroidal rotation scan experiment from the JT-60U in the pre-FSTs campaign is overlaid only for a configuration having small plasma volume ($V_p \sim 50 \text{ m}^3$). As well, the database from the JT-60U in the post-FSTs campaign is plotted in cross (red) symbols for the small $V_p \sim 50 \text{ m}^3$ configuration in the co-NBI (plus perp.-NBI) discharges. (b) The database of $\Delta W_{ELM}/W_{ped}$ in the toroidal rotation scan experiments from the JT-60U in the pre-FSTs campaign is overlaid only for a configuration having large plasma volume ($V_p \sim 75 \text{ m}^3$). As well, the database from the JT-60U in the post-FSTs campaign is plotted in box-plus (green) symbols for large $V_p \sim 75 \text{ m}^3$ configurations in co-NBI (plus perp.-NBI) discharges.

regime. Returning to Fig. 13 (a), the international database is also overlaid with the result of rotation scan experiments on the JT-60U at the pre-FSTs campaign, scanning the direction of the momentum injection from co-, balanced-, and counter-directions at a fixed collisionality of around $\nu_e^* \sim 0.3 \pm 0.1$ in a small volume plasma of $V_p \sim 50 \text{ m}^3$. In the case of co-NBI, an ‘‘averaged’’ normalized ELM energy loss, $\langle \Delta W_{ELM}/W_{ped} \rangle$, is around 10.5%. The balanced case indicates a somewhat smaller $\langle \Delta W_{ELM}/W_{ped} \rangle \sim 9\%$ than the co-NBI case. Furthermore, the counter-NBI case indicates the smallest $\langle \Delta W_{ELM}/W_{ped} \rangle \sim 6.6\%$, reaching the ITER’s maximum tolerable ELM size, though the results of rotation scans of the small volume plasma recover only the collisionality scaling seen on other machines within their ranges of variability.

Figure 13 (b) shows another experimental result of rotation scan experiments on the JT-60U at the pre-FSTs campaign, scanning the direction of the NBI from co-, balanced-, and counter-directions at a fixed collisionality of around $\nu_e^* \sim 0.3 \pm 0.1$ in a large volume plasma of $V_p \sim 75 \text{ m}^3$. As described in Sec. 3.2, the large volume case indicates a very small ELM energy loss of less than the ITER’s maximum tolerable ELM size, varying from a $\Delta W_{ELM}/W_{ped} \sim 2.5\%$ to 6.7%, indicating that the collisionality relationship could be broken. So again, the extrapolation of the ELM energy loss based on present experiments to the ITER remains uncertain.

An improved pedestal pressure through the use of FSTs, which is presented clearly in Ref. [14], makes it possible to access to the lower ν_e^* regime at a large plasma volume as shown in Fig. 13 (b) (box-plus symbols). However, the normalized ELM energy loss, $\Delta W_{ELM}/W_{ped}$ is found still to be very small, i.e., less than the ITER’s maximum

tolerable ELM size even at the ν_e^* close to that expected in the ITER. On the other hand, as shown in Fig. 13 (a), the absence of remarkable differences between the pre- and the post-FST campaign seen in the small volume plasma may be reasonable, since the TF-ripple in the inward-shifted configuration for both the pre- and the post-FST campaign is as small as those in other tokamaks. In this configuration having a small TF-ripple, ELMs and pedestal characteristics could not be strongly affected by the losses of the fast ions from perpendicular NBI. These new findings suggest that the TF-ripple itself may not directly affect the normalized ELM energy loss, $\Delta W_{ELM}/W_{ped}$, and plasma configuration as well as toroidal rotation at the plasma edge appear important to the prediction of ELM size in future devices. The effects of other parameters, such as plasma elongation κ or triangularity δ , the height of the X-point from the divertor plate, and the distance between the plasma and wall Δ_{SEP} , should be carefully considered along with an accurate ELM model (e.g., the edge stability analysis code of the ‘‘peeling-ballooning’’ mode including the effects of plasma shaping and rotation), which is constrained by high precision fast temporal measurements.

5. Summary and Discussion

The results of systematic study of Type-I ELM characteristics in tangential co-, balanced-, and counter-NBI plus perpendicular NBI heated plasmas in various configurations confirmed that the ELM energy loss, ΔW_{ELM} , is strongly related to the toroidal rotation at the plasma edge, $v_{T,ped}$, while the energy stored in the pedestal, W_{ped} , shows weak dependence on $v_{T,ped}$, and hence we could control the normalized ELM energy loss, $\Delta W_{ELM}/W_{ped}$, by means of

counter-NBI as summarized in the Table 1. In addition, not only $v_{T,ped}$, but also the configuration correlates with $\Delta W_{ELM}/W_{ped}$, indicating that the reduction in ΔW_{ELM} is larger than that seen in W_{ped} , and hence $\Delta W_{ELM}/W_{ped}$ decrease when plasma volume increases. Furthermore, the similar dependences of the $\Delta W_{ELM}/W_{ped}$ on the $v_{T,ped}$ as seen in a comparison of the pre- and the post-FSTs campaigns, which is due to the increase in both ΔW_{ELM} and W_{ped} according to the enhanced $v_{T,ped}$ in the co-direction, suggest that plasma configuration plays a more important role than δ_{ripple} in the appearance of small Type-I ELM in large volume plasma, and the TF-ripple itself and/or losses of fast ions may not directly affect the normalized ELM energy loss, $\Delta W_{ELM}/W_{ped}$. It is noted that change in the δ_{ripple} after installation of FSTs is not simply defined by the standard definition ($\equiv [(B_{t,max} - B_{t,min})/2]/B_{t,ave}$), but is evaluated in terms of the toroidal variation of the toroidal magnetic field strength at a certain location in the poloidal cross section due to the complex structure of the toroidal filed ripple as shown in Fig. 14. Here, $B_{t,max}$, $B_{t,min}$, and $B_{t,ave}$ are the maximum, minimum and averaged values of the toroidal magnetic field, respectively.

The development of an ELM mitigation technique is critical for the design of future large tokamaks such as the ITER. ELM mitigation has been demonstrated in the JT-60U counter-NBI discharge in the configuration having small plasma volume, but its application to the ITER condition is uncertain, since the energy confinement enhancement factor relative to H-mode scaling, $H98(y, 2)$ [19], in the counter-NBI discharge is somewhat less than that of the co-NBI discharge [14]. So, further quantitative assessment, including local control of the v_T or its shear in the plasma's edge region, is required for the development of a

robust ELM control method, which is compatible with the greater energy confinement in the plasma's core region. In addition, compared to other tokamaks, the v_e^* -scaling of $\Delta W_{ELM}/W_{ped}$ is favorable in the JT-60U with this configuration having a larger plasma volume. As discussed in Ref. [20], the plasma-shaping effect may account for the appearance of small Type-I ELMs even at around $v_e^*_{ITER}$

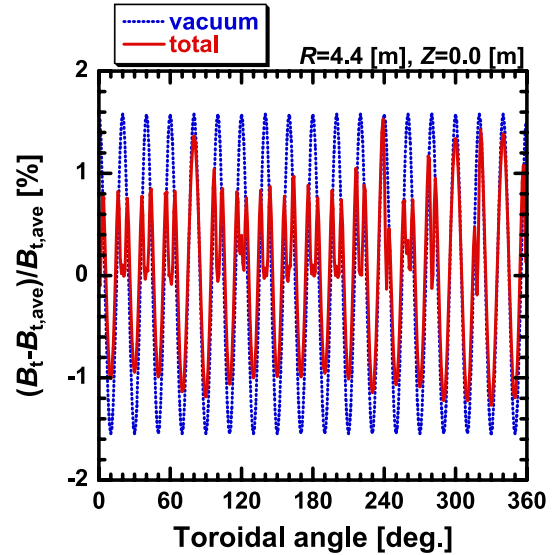


Fig. 14 Toroidal variation of the ratio of the toroidal magnetic field strength to the averaged one after the installation of the FSTs at $R = 4.4$ m and $Z = 0.0$ m for a configuration having large volume plasma (see Fig. 11) with the toroidal magnetic field on axis $B_{t,axis} = 2.6$ T shown by percentage. A solid line is the total toroidal magnetic field and a dotted line is the vacuum magnetic field.

Table 1 Characterization of the present qualitative understanding of ELMs and the pedestal. Note that a degree of each slope could compare only a certain vertical line, and a comparison within a same horizontal line makes no sense.

	$v_{T,ped}$ ctr→bal→co	δ_{ripple} 1%*→2% (with →w/o FSTs)	Configuration small→middle→large ($V_p \sim 50 \text{ m}^3 \rightarrow 65 \text{ m}^3 \rightarrow 75 \text{ m}^3$)
ΔW_{ELM}	↗	↘	↘
W_{ped}	↗	↘	↘
$\Delta W_{ELM}/W_{ped}$	↗	→	↘

(*) Change in the δ_{ripple} after installation of FSTs is not simply defined by the standard definition ($\equiv [(B_{t,max} - B_{t,min})/2]/B_{t,ave}$), but is evaluated in terms of the toroidal variation of the toroidal magnetic field strength at a certain location in the poloidal cross section due to the complex structure of the toroidal filed ripple as shown in Fig. 14. Here, $B_{t,max}$, $B_{t,min}$, and $B_{t,ave}$ are the maximum, minimum and averaged values of the toroidal magnetic field, respectively.

in a large volume plasma, especially on the post-FSTs campaign. Future studies, including an edge stability analysis employing the MARG2D code developed in [21], will be directed towards further revealing the effect disclosed by large changes in the plasma configuration.

Acknowledgments

The authors are much indebted to the whole JT-60 team for their support. Thanks are also due to Drs. M. Kikuchi, T. Fujita, T. Ozeki, M. Nagami, and T. Takizuka for their continuous encouragement. A special thanks goes to Dr. G. Matsunaga for his extraordinary effort to illustrate with the top view of the JT-60U.

- [1] ITER Physics Basis, Nucl. Fusion **39**, 2175 (1999).
- [2] A. Loarte *et al.*, Nucl. Mater. **313-316**, 962 (2003).
- [3] T.E. Evans *et al.*, Phys. Rev. Lett. **92**, 235003 (2004).
- [4] H. Urano *et al.*, Plasma Phys. Control. Fusion **45**, 1571 (2003).
- [5] A.W. Degeling *et al.*, Plasma Phys. Control. Fusion **45**, 1637 (2003).
- [6] C.M. Greenfield *et al.*, Phys. Rev. Lett. **86**, 4544 (2001).
- [7] W. Suttrop *et al.*, Plasma Phys. Control. Fusion **46**, A151 (2004).
- [8] Y. Sakamoto *et al.*, Plasma Phys. Control. Fusion **46**, A299 (2004).
- [9] N. Oyama *et al.*, Nucl. Fusion **45**, 871 (2005).
- [10] Y. Kamada *et al.*, Plasma Phys. Control. Fusion **44**, A279 (2002).
- [11] Y. Koide *et al.*, Plasma Phys. Control. Nucl. Fusion Res. **1**, 777 (1992).
- [12] M. Yoshida *et al.*, Plasma Phys. Control. Fusion **48**, 1673 (2006).
- [13] H. Urano *et al.*, Plasma Phys. Control. Fusion **48**, A193 (2006).
- [14] H. Urano *et al.*, *Proc. 21st IAEA Fusion Energy Conf.*, Chengdu (China), 2006, appear in CD-ROM paper IAEA-CN-149/EX/5-1.
- [15] K. Shinohara *et al.*, *Proc. 21st IAEA Fusion Energy Conf.*, Chengdu (China), 2006, appear in CD-ROM paper IAEA-CN-149/FT/P5-32.
- [16] P.B. Snyder *et al.*, Plasma Phys. Control. Fusion **46**, A131 (2004).
- [17] G. Federici *et al.*, Nucl. Mater. **313-316**, 11 (2003).
- [18] G. Federici *et al.*, Plasma Phys. Control. Fusion **45**, 1523 (2003).
- [19] J.G. Cordey *et al.*, Plasma Phys. Control. Fusion **39**, B115 (1997).
- [20] P.B. Snyder *et al.*, Nucl. Fusion **44**, 320 (2004).
- [21] N. Aiba *et al.*, *Proc. 21st IAEA Fusion Energy Conf.*, Chengdu (China), 2006, appear in CD-ROM paper IAEA-CN-149/TH/P8-1.